*Journal of Applied Fluid Mechanics*, Vol. 17, No. 6, pp. 1204-1216, 2024.
Available online at www.jafmonline.net, ISSN 1735-3572, EISSN 1735-3645.
https://doi.org/10.47176/jafm.17.6.2329

# Simulation of Non-Newtonian Blood Flow in Diverging Bifurcated Vessels

J. Chu[1], L. L. Xiao[†1], C. S. Lin[2], S. Liu[3], K. X. Zhang[4] and P. Wei[3]

[1] *School of Mechanical and Automotive Engineering, Shanghai University of Engineering Science, Shanghai, China*
[2] *Artificial Intelligence Innovation and Incubation Institute, Fudan University, Shanghai, China*
[3] *School of Aerospace Engineering and Applied Mechanics, Tongji University, Shanghai, China*
[4] *School of Medicine, Nankai University, Tianjin, China*

†*Corresponding Author Email: xiaoll_sues@sues.edu.cn*

## ABSTRACT

Bifurcated vessels represent a typical vascular unit of the cardiovascular system. In this study, the blood flow in symmetric and asymmetric bifurcated vessels are simulated based on computational fluid dynamics method. The blood is modeled as non-Newtonian fluid, and the pulsatile flow velocity is applied on the inlet. The effects of the fluid model, bifurcation angle and symmetry of the geometry of the vessel are investigated. The results show that the wall shear stress (WSS) on the outer wall of daughter branches for the non-Newtonian fluid flow is greater than that for Newtonian fluid flow, and the discrepancy between the flow of two fluid models is obvious at relatively low flow rates. With the bifurcation angle increases, the peak axial velocity of the cross-section of daughter branch decreases, so the WSS increases. For the non-Newtonian fluid flow in the asymmetric bifurcated vessels, more flow passes through the daughter vessel with a lower angle, and the WSS along the outer wall of which is lower. Furthermore, the region with a low time-averaged wall stress (TAWSS) and high oscillating shear index(OSI) distributed on the outer wall of bifurcation vessels are larger for the flow in the vessel with smaller bifurcation angle. In conclusion, the effects of the blood viscosity cannot be neglected at low flow rates and the geometry of the bifurcated vessel plays a key role with regards to the blood flow.

***Article History***

*Received September 24, 2023*
*Revised December 11, 2023*
*Accepted January 4, 2024*
*Available online March 27, 2024*

***Keywords:***

*Blood flow*
*Non-Newtonian*
*Bifurcated vessel*
*Wall shear stress*
*CFD*

## 1. INTRODUCTION

Flow bifurcations, such as multiple bronchial bifurcations in the respiratory system and blood and lymph flow through blood vessels, are widespread in the human body (Arjmandi & Razavi, 2012; Beier et al., 2016; Abugattas et al., 2020). Blood carries oxygen as well as nutrients to various tissues in the body through the circulatory system, and the bifurcation structure is the most common blood vessel in the cardiovascular system (Zhao et al., 2000; Chen et al., 2020). The behavior of blood flow is strongly influenced by the geometry of vessels, and complex flow fields can lead to vascular disease (Spanos et al., 2017) . Several studies have shown complex flow behavior at vascular bifurcations (Soares et al., 2021; Harris et al., 2023). Therefore, it is important to study the flow behavior of blood in bifurcated vessels.

Atherosclerosis is a vascular lesion characterized by atherosclerotic damage to the arterial lining and is one of the underlying causes of cardiovascular disease (Kucharska-Newton et al., 2017). Currently, it is believed that the formation of atherosclerosis is related to the permeability of endothelial cells in the vascular wall (Libby et al., 2011). Studies have shown that arterial stenosis leads to abnormal hemodynamic parameters and damage to the inner wall of the vessel, which in turn induces atherosclerosis (Caro et al., 1969; Fry, 2002; Nagargoje et al., 2021; Kamangar, 2022). Thus, the WSS provides important information for predicting which regions develop atherosclerosis. However, trying to obtain accurate approximate WSS values is complicated. Some researchers have obtained velocity fields by particle image velocimetry (PIV) and magnetic resonance fluid dynamics (MRI) techniques and computed the WSS by calculating the velocity field is more accurate (Cox et al., 2019), but it requires the assistance of equipment; therefore, it is more convenient to use a purely computational method to obtain the WSS. Some scholars have experimentally verified the accuracy of using numerical simulation to

calculate the WSS (Bordones et al., 2018; Cox et al., 2019).

The arterial bifurcation vessel has a greater impact on blood flow due to the bifurcation angle (Zhang & Dou, 2015). For instance, Liu et al. (2015) found that in the right coronary artery, the angle of the side branch had a significant effect on atherosclerotic lesions. However, Beier et al. (2016) compared the results of stented and non-stented Y-bifurcation vessels and concluded that the bifurcation angle had little effect on hemodynamics. Chaichana et al. (2011) investigated various combinations of bifurcation angles and low wall shear stress gradient was demonstrated with wide angles. The nonplanarity of bifurcation vessels is an important factor in hemodynamics and may play a significant role in pathophysiology (Chen & Lu, 2004, 2006). Nagargoje (Nagargoje & Gupta, 2020; Nagargoje et al., 2021) constructed symmetric and asymmetric bifurcation vessels, demonstrated that the flows of Newtonian and non-Newtonian fluids are obviously different in these vessels and observed a pair of helical vortices near the bifurcation.

Blood is a suspension composed primarily of blood cells and plasma, of which red cells make up more than 40% of the blood volume (Xiao et al., 2020a, 2023). Interactions among the red cells lead to complex rheological behavior (Freund, 2014). Blood viscosity does not significantly change at high shear rates, and at low shear rates, cell-to-cell adhesion increases, leading to an increase in blood viscosity (Xiao et al., 2020a, 2021), which is a well-known non-Newtonian characteristic (Kannojiya et al., 2021). In the cardiovascular network, blood is affected by the vascular structure and the pulsatile flow in a cardiac cycle. Therefore, it is important to adopt a non-Newtonian fluid model to characterize the blood flowing through bifurcating vessels. Caballero and Laín (2014) studied steady-state blood flows in human thoracic aortic vessels and compared Newtonian and non-Newtonian rheological behaviors, suggesting that the Newtonian assumption is a good approximation at medium and high flow rates (the shear rate is higher than $100S^{-1}$). Abugattas (2020) employed the Power Law, Cross and Carreau-Yasuda viscosity models of the carotid artery to study the bifurcation flow behavior of non-Newtonian fluid in the vessel and concluded that different non-Newtonian models have different wall shear stresses in geometric stress concentrations. With the development of computer techniques and numerical methods, blood flow under physiological conditions can be simulated.

In most of the previous studies on blood flow, specific bifurcated vessels were focused on, and the non-planarity and asymmetry of the vessels have been analyzed in some studies. Few studies on how the bifurcation angle affects the blood flow behavior and atherosclerotic areas have been reported. In this study, the blood flow in three-dimensional bifurcated arteries is simulated. The effects of the rheological model, bifurcation angle and symmetry of bifurcation on the blood flow and vulnerable areas are investigated. Some conclusions drawn from this work are made, aiming to provide theoretical insight into the blood flows in bifurcating vessels.

## 2. MODELS AND METHODS

### 2.1 Model Geometry and Parameter Values

In this article, the geometrical models considered are based on the model used by Chen and Lu (2004, 2006). as shown in Fig.1. The diverging bifurcated vessel consists of the mother vessel and two daughter branches. Each branch forms an angle with the parent vessel, termed the bifurcation angle α and bifurcation angle β. The length of the mother vessel is 3 times its diameter d. The length of the daughter branch is 8d. Referring to Perktoid's data and individual differences in arterial vessels, the arterial vascular diameter(d) is assumed to be 6mm (Arjmandi & Razavi, 2012). A smooth curved transition is considered at the connection between the blood vessels. The diverging bifurcations can be considered symmetric and asymmetric, according to achieved by changing the distribution of the bifurcation angles. The distribution of the bifurcation angles is given in Table 1.

### 2.2 Governing Equation and Rheological Model

The blood flowing through the idealized arterial bifurcated vessel is considered to be pulsatile, laminar, and incompressible. The control equations are spatially discretized using the finite volume method, the SIMPLE algorithm is applied to solve the coupled pressure-velocity discretization equations, and a second-order upwind scheme is used for the momentum equations. The flow

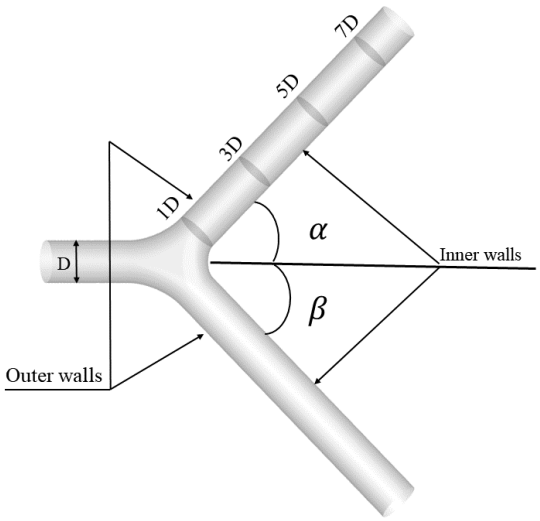


**Fig. 1 Schematic diagram of the diverging bifurcated vessel model**

**Table 1 Various bifurcation angle combinations**

| Sr.No | Case | Angle |
|---|---|---|
| 1 | Symmetric | $\alpha = \beta = 30°$ |
| 2 | | $\alpha = \beta = 45°$ |
| 3 | | $\alpha = \beta = 60°$ |
| 4 | Asymmetric | $\alpha = 45°,\ \beta = 15°$ |
| 5 | | $\alpha = 45°,\ \beta = 30°$ |
| 6 | | $\alpha = 45°,\ \beta = 60°$ |

governing equation is based on three-dimensional Naiver–Stokes equations, which are given by:

$$\nabla \cdot u = 0 \tag{1}$$

$$\rho\left(\frac{\partial u}{\partial t} + u\left(u \cdot \nabla\right)\right) = -\nabla P + \nabla \cdot \tau \tag{2}$$

Here, U is the velocity vector, $\rho$ is the density of blood, and $p$ is the pressure. $\tau$ is the stress tensor and can be represented by:

$$\tau = 2\mu\left(\dot{\gamma}\right)D \tag{3}$$

$\mu$ is the apparent viscosity of the fluid. The rate of deformation tensor D is defined as

$$\mathrm{D} = \frac{1}{2}\left(\nabla u + \nabla u^{T}\right) \tag{4}$$

$\dot{\gamma}$ represents the shear rate, it can be given by Equation (5)

$$\dot{\gamma} = \sqrt{\frac{1}{2}D : D} \tag{5}$$

At relatively low flow rates, interactions between red blood cells are enhanced and blood will exhibit non-Newtonian properties. In this paper, the Carreau-Yasuda viscosity is numerically calculated to describe the shear-thinning behavior of blood, which is implemented using user-defined functions(UDF) in FLUENT and can be written as given by Eq.(6)

$$\eta = \mu_{\infty} + (\mu_0 - \mu_{\infty})\left[1 + \left(\lambda\dot{\gamma}\right)^{b}\right]^{\frac{a-1}{b}} \tag{6}$$

The term $\eta$ denotes dynamic viscosity, and $\dot{\gamma}$ denotes the shear rate. The parameters in Eq.(6) are obtained from the literature and expressed as follows: the high shear viscosity is $\mu_{\infty} = 0.056$ Pa·s, low shear viscosity is $\mu_0 = 0.00345$ Pa·s, the relaxation time is $\lambda$ =1.902, and the power law indices $a$ and $b$ are 0.22 and 1.25, respectively (Weddell et al., 2015). A typical Newtonian viscosity value of $\mu = 0.0035$ Pa·s is considered. Figure 2 shows the viscosity for different models. The Carreau model and whole blood data from the literature were used(Kelly et al., 2020). The Carreau-Yasuda model fits well with other non-Newtonian models. The density of blood is 1050 kg/m$^3$(Johnston et al., 2004).

### 2.3 Boundary Conditions and Hemodynamics Parameter

Due to intermittent blood supply to vessels by the heart. the blood flow in the artery is pulsatile. Similar to chen et al. (2020) a time-varying velocity modeled by a fitting curve for the carotid artery is applied at the entrance of the main vessel, as shown in Fig. 3.

$$\mathrm{V_{inlet}} = \begin{cases} 0.2+25t^2 & 0 \le t \le 0.08 \\ -0.1008+8.32t-32t^2 & 0.08 < t \le 0.2 \\ 0.7888-3.792t+6.32t^2 & 0.2 < t \le 0.36\,(s) \\ 1.10463232-3.933184+4.2752t^2 & 0.36 < t \le 0.46 \\ 0.2 & 0.46 < t \le 0.8 \end{cases}$$

The duration of a cardiac cycle is about approximately 0.8s, during which the blood flows at some particular instants of time, such as at $T_1$=0.13*s* (peak systolic), $T_2$=0.2*s* (deceleration) and $T_3$=0.7*s* (end of diastole). At $T_1$, the blood flow rate reaches the maximum value of 0.44m/s, corresponding to Re=803.48, which is far from the lower critical value of turbulent flow. Thus the adopted laminar flow model is reasonable. The outflow is imposed on the outlet of the two branch vessels. A non-slip boundary condition is applied to the inner wall of all vessels.

The region with low or oscillating WSS for a long time is regarded as the susceptible region of atherosclerosis, and the instantaneous parameters cannot be directly used to describe the magnitude and oscillation of WSS for the whole cycle, Therefore, it is also necessary to determine the eligible susceptible region by time-averaged analysis. In this paper, the TAWSS and OSI,

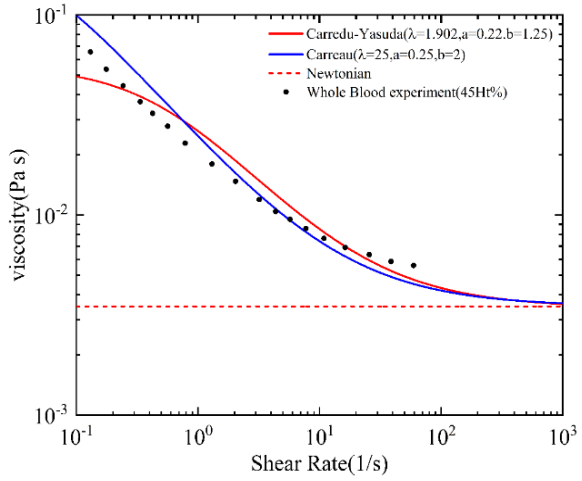


**Fig. 2 Viscosity curve for the Carreau-Yasuda and other blood models**

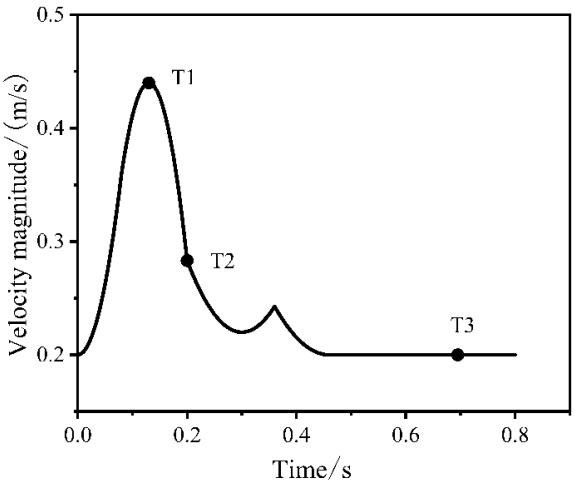


**Fig. 3 Pulsatile axial velocity imposed on the inlet of the parent vessel in a cardiac cycle**

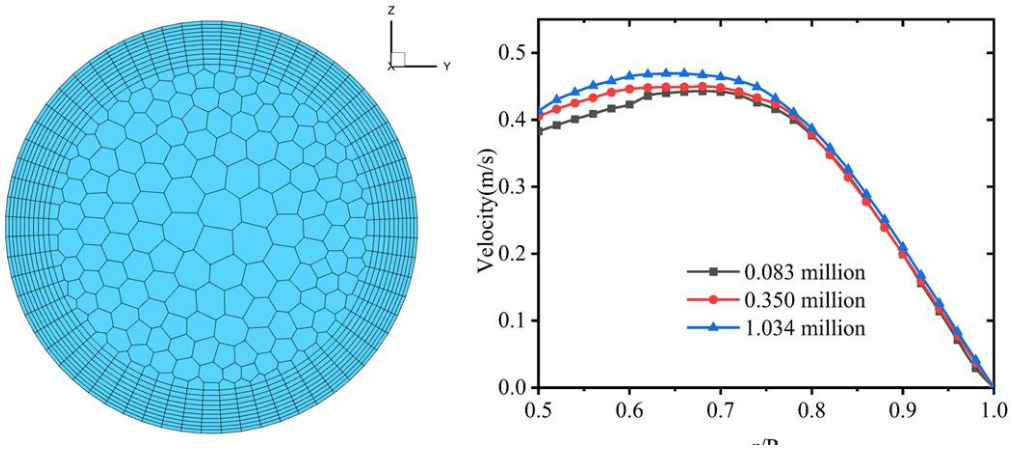


(a) (b)

**Fig. 4 (a) Mesh at the inlet (b) Comparison of the velocity with three different mesh densities**

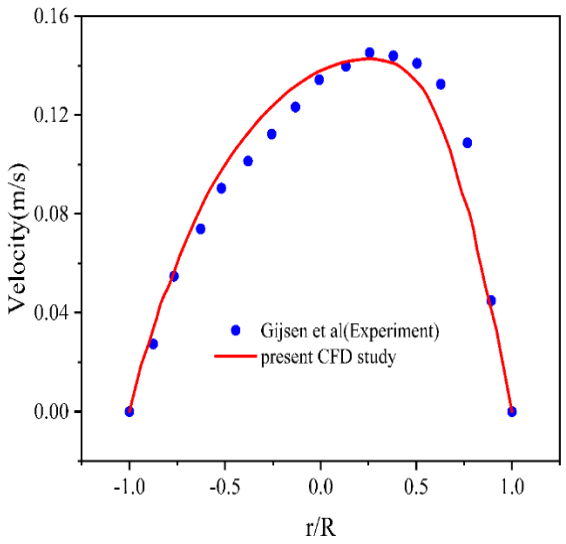


**Fig. 5 Comparison of the experimental axial velocity results.**

which were commonly used in previous studies, were selected for analysis. The two parameters are calculated as follows:

$$TAWSS = \frac{1}{T}\int_0^T |WSS|dt \tag{7}$$

Where $T$ is the time of one cardiac cycle.

$$OSI = 0.5\left[1 - \frac{\left|\int_0^T WSSdt\right|}{\int_0^T |WSS|\,dt}\right] \tag{8}$$

The OSI is a nondimensional parameter whose value varies between 0 and 0.5. The role of the OSI is to characterize oscillations in the WSS direction during a cardiac cycle, with larger values indicating more severe oscillations.

### 2.4 Mesh Independence Study and Validation

In most simulations of arterial hemodynamics, the velocity gradient near the wall has always been an important factor affecting the accuracy of the simulation results. Therefore, to ensure that the results are grid-independent, a grid for Hexcore-poly with ten layers of inflation is generated by FLUENT MESHING, as shown in Fig. 4(a). The three different grid densities were set for comparison. Figure 4(b) shows the profile of the velocity obtained using three different meshes at a line located on the bifurcation plane at a distance of 2D from the bifurcation. It is clear that the solution differences are less than 1% for the two meshes(0.350 and $1.034 \times 10^6$elements). Hence, the mesh parameters were set to be the same as the number of grids $0.350 \times 10^6$ million.

The current numerical results were verified by comparison with experimental data from the literature (Gijsen et al., 1999), which provide experimental results for non-.Newtonian flow in a 90º-bend tube. The axial velocity profiles were compared on the 45º plane, as shown in Fig. 5. The numerical results are in good correspondence with the experimental results.

## 3. RESULTS AND ANALYSIS

### 3.1 Flow of Blood in the Bifurcated Vessels

When blood flows through the diverging zone, its flow field changes dramatically. Figure 6(a) shows the contour of velocity on the bifurcation plane of the symmetric bifurcated vessels (α=β=45º). The blood flow passes through the bifurcation and is separated into two branching vessels. It can be seen from the figure that the distribution of velocity in both branching vessels is symmetric, due to the symmetry of the bifurcation geometry. It is faster at the inner wall close to the branching canal with a narrow section of the velocity maxima region, and a low-velocity region with a larger area appears on the side away from the inner wall. In addition, the blood flow is disrupted by the bifurcation and recirculation zones, where the streamlines exhibit unique helical flow patterns, as shown in Fig. 6(b). As the blood flows downstream of the branch, the flow velocity gradually slows down.

The axial velocity profiles in the bifurcation plane along the daughter vessel are shown in Fig. 7. The non- dimensional radius $r$/R=1 denotes the outer wall of

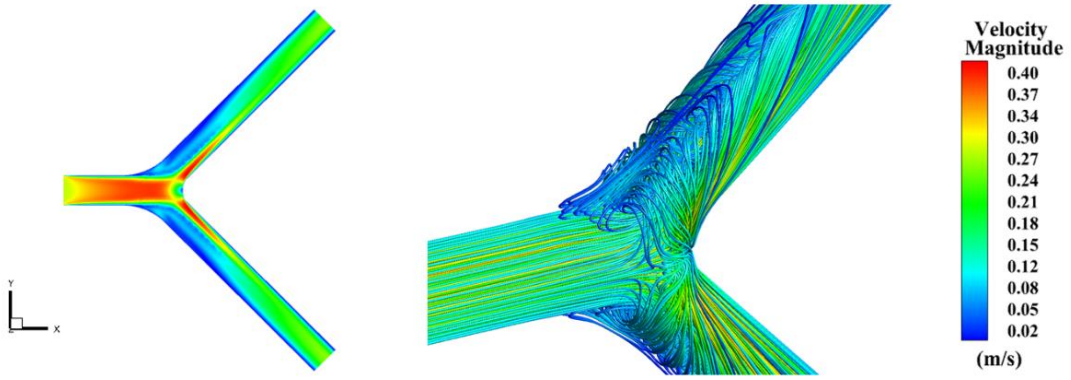


(a) (b)

**Fig. 6 Contours of the velocity on the bifurcation plane for the symmetric bifurcation angles α = β = 45º and velocity streamlines at deceleration.(a) Contour of the velocity (b) Velocity streamline contours**

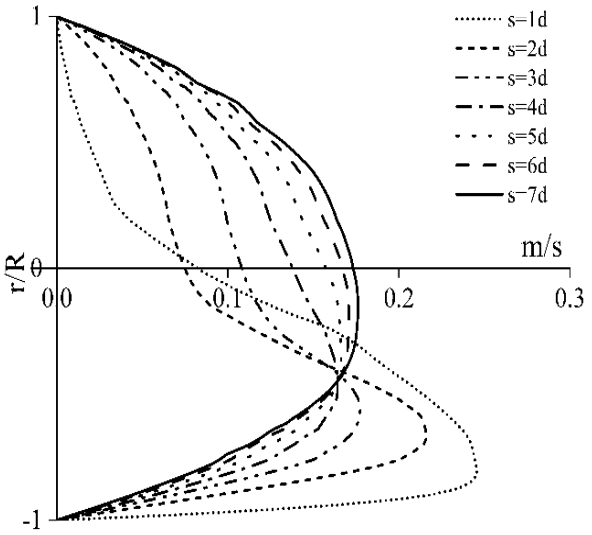


**Fig. 7 Profiles of the axial velocity on the bifurcation plane in the daughter vessel at *S*=1d~7d for the symmetric bifurcation angles α = β = 45º at the end of the diastole**

the vessel and *r*/R=-1 represents the inner wall of the vessel. *S* is the distance along the axis from the location of the cross-section through the conjunction of the two branches. The low-velocity zone occurs on the outer walls of the vessels near the entry segment of the daughter branches, indicating that flow reversal formed near the outer vascular walls in the region of *S* = 1d. Downstream of the bifurcation, the velocity profiles flatten at *S*=6d and *S*=7d, which indicates that the flow field is fully developed.

Figure 8 shows the velocity contours and secondary flow streamlines along the daughter vessel at the peak systole. Obviously, the contours of the axial velocity are skewed to the inner wall near the branch point, but a nearly parabolic velocity profile can be seen near the exit of the branch. The movement of fluid from the outer wall to the inner wall is observed, resulting from a centripetal acceleration or the pressure gradient introduced by the curvature of the bifurcation. Counterrotating vortices, which are also called Dean vortices, occur at the cross sections close to the bifurcation. These vortices cause a shift of the peak axial velocity toward the inner wall.

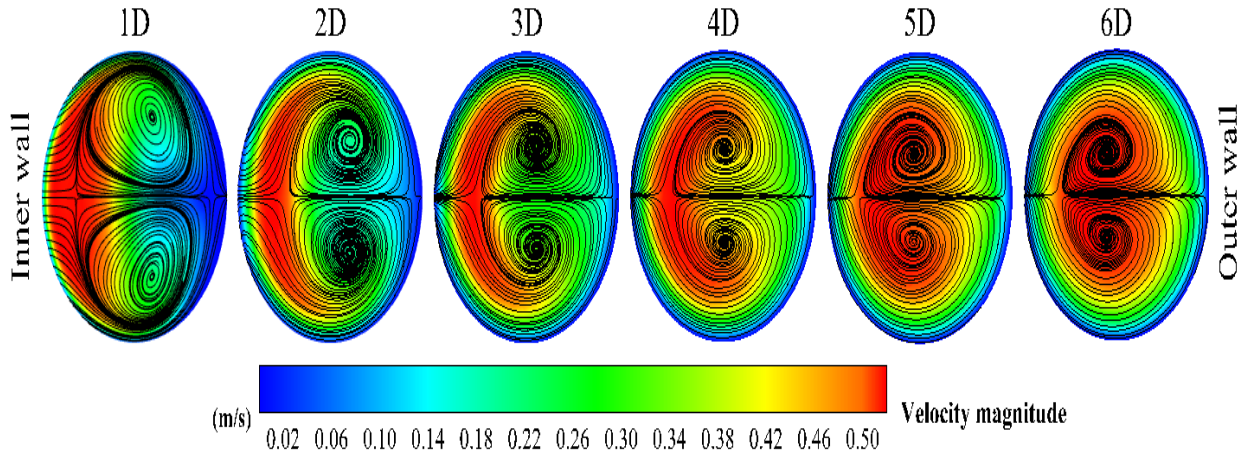


**Fig. 8 Contours of the velocity and secondary flow streamlines on the cross-sectional planes in the daughter branch at *S*=1d~6d**

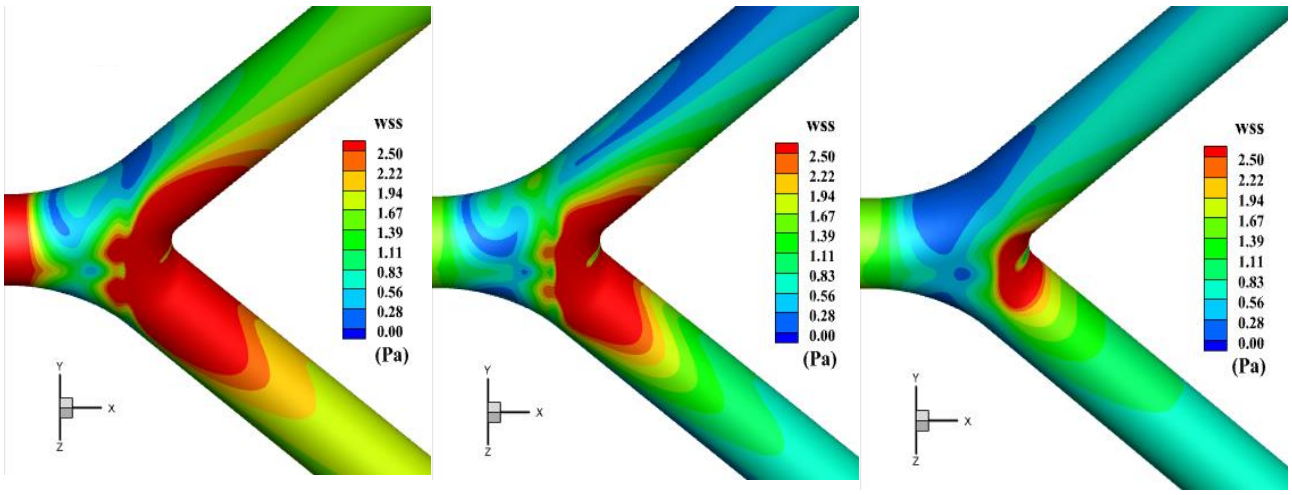


(a) (b) (c)

**Fig. 9 Contours of the wall shear stress on the vascular walls of the bifurcation at three different moments: (a)*t* =$T_1$, (b)*t* =$T_2$, and(C)*t* =$T_3$**

Figure 9 is the contour plot of the WSS on the vascular walls. The WSS on the inner wall is higher than that on the outer wall near the conjunction of two daughter branches. This is a result of the high-velocity gradient near the inner wall of the bifurcation (as shown in Fig. 6(a) or Fig.7), due to the presence of the bifurcation. It also shows that with the decrease in the mean velocity, the WSS along the vessel wall experiences a downward trend. This is due to the thicker viscous boundary layer near the inner wall of the bifurcation, as shown by comparing Figs. 9(a)~(c).

### 3.2 Effects of the Non-Newtonian Behaviors of Fluid Flows in Bifurcated Vessels

The blood exhibits shear thinning behavior at relatively low shear rates, which often occurs at the flow separation regions in the bifurcated vessels. It is necessary to incorporate the non-Newtonian fluid properties. Figure 10 presents the distributions of the WSS along the outer wall and inner wall of the bifurcation plane of the symmetric bifurcated vessel with $\alpha = \beta = 45^o$. The results show that a significant difference in the WSS exists for non-Newtonian and Newtonian flows, especially along the outer wall. In Fig.10c, the average difference in the WSS for non-Newtonian flow is 0.95% higher than that for Newtonian flow. Additionally, the profiles of the WSS on the daughter vessels at the peak systole and at the end of diastole are similar. In addition, the magnitudes of the WSS at the peak systole are much higher, resulting from the larger mean velocity and thinner viscous boundary layer. Moreover, the WSS reaches its peak on the inner wall near the entry section of the daughter vessel. As the flow separation occurs at the region where the WSS is approximately 0, it can be seen that the WSS at the peak systole and end of the diastole on the outer wall near the entry section of the daughter vessels reaches its valley value, close to 0. Notably, the profiles of the WSS for non-Newtonian flows are higher than those for Newtonian flow at relatively low flow velocies, and the non-Newtonian property of blood cannot be neglected.

To understand the effects of the rheological model on flow phenomena, the secondary vortex at *S*=1D, 3D, 5D and 7D for the symmetric bifurcated vessel with $\alpha=\beta=45^o$ at the end of the diastole, is shown in Figure 11. A pair of vortices with opposite rotational directions are observed at *S*=1D-5D. These vortices are known as Dean vortices. It is obvious that the structure of the rotational vortices for the non-Newtonian fluid breaks down, but that for the Newtonian fluid exists at *S*=7d. This phenomenon occurs because the shear-thinning fluid exhibits higher viscosity under a low shear rate, which further reduces the flow velocity of the non-Newtonian fluid in the daughter branch. Compared to the velocity for Newtonian fluid flows in the daughter vessel, the velocity for non-Newtonian fluid flows is lower , and it is easy to reach the fully developed flow formed downstream.

### 3.3 Effects of The Bifurcation Angle on Blood Flow in Symmetric Bifurcated Vessels

To determine how the bifurcation angle affects the blood flow phenomena, the profiles of the axial velocity and WSS along the daughter vessels in the bifurcation plane for the non-Newtonian fluid flow during the peak systole are analyzed. Figure 12 demonstrates the profiles of axial velocity for three bifurcation angles at locations *S*=1d~6d. As shown in Fig 12(a), the flow separation, indicated by negative values of the axial velocity, is formed on the outer walls of the vessels near the bifurcation at *S*=1d. Under the influence of the flow reversal, the axial velocity near the inner wall increases with the bifurcation angle, as shown in Fig.11(a). Moreover, downstream of the daughter vessels, the peak value of the axial velocity is smaller for the larger bifurcation angle at *S*=3d~6d.

Figure 13 shows the distributions of the WSS along the outer and inner walls on the bifurcation plane of the three symmetric daughter vessels at the peak diastole. As seen in Fig.13(a), the WSS along the outer wall is 0 for $\alpha = \beta = 30^o$, $45^o$ and $60^o$ at S=1.5. This implies that with the increase in the bifurcation angle, flow separation occurs earlier downstream of the branching vessel. Moreover, the WSS along the downstream of the daughter vessel increases as the bifurcation angle increases. The WSS gets closer to the value for fully-developed flow in a shorter distance for the bifurcated vessel with a larger bifurcation

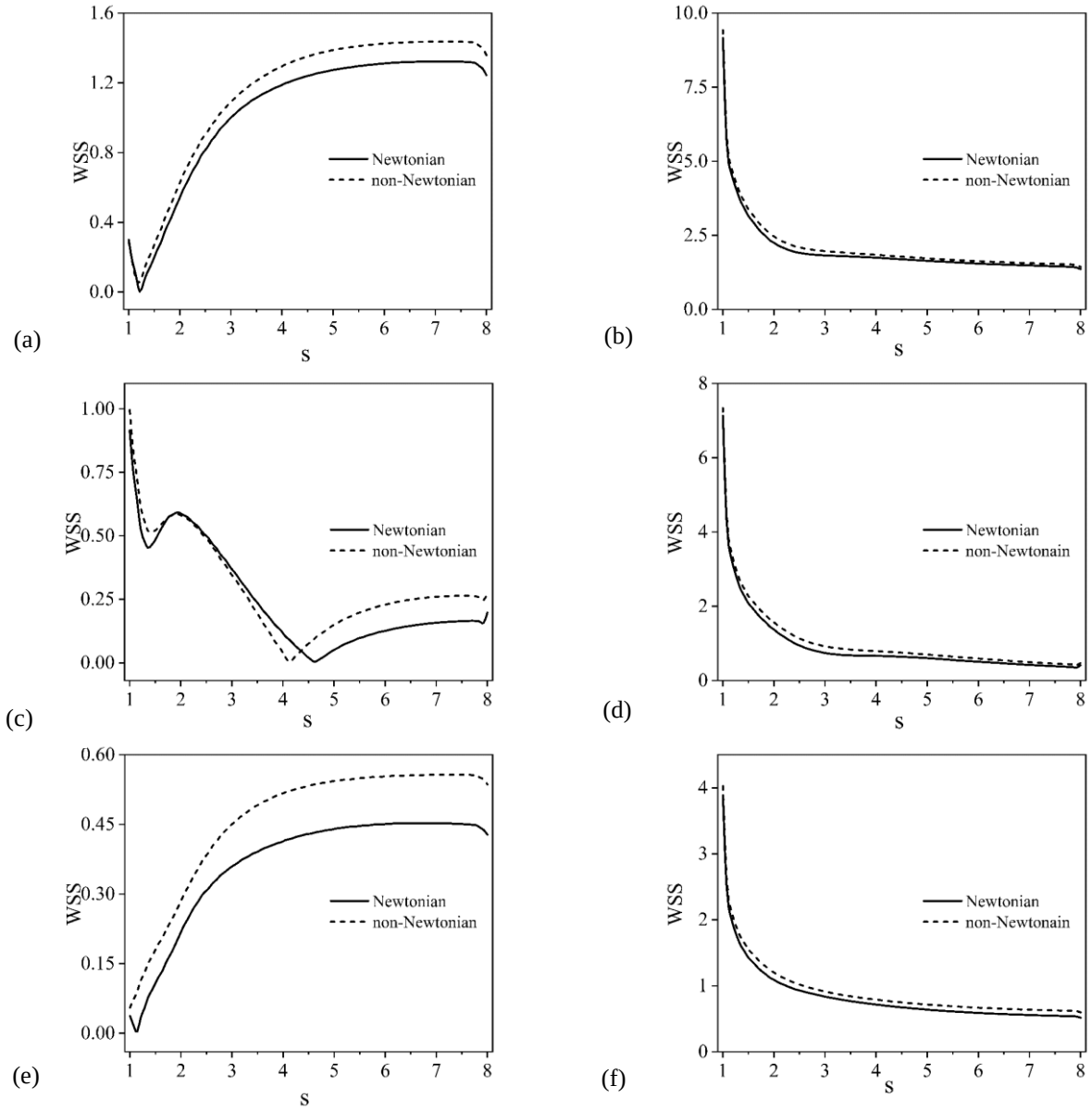


**Fig. 10 Distributions of the WSS along the outer wall at (a) $t$=$T_1$ (the peak systole), (c)$t$=$T_2$ (the beginning of the diastole), and (e)$t$=$T_3$ (the end of the diastole)as well as the inner wall at (b) $t$=$T_1$, (d) $t$=$T_2$ and (f) $t$=$T_3$ on the bifurcation plane of the daughter vessel for the flow in the symmetric bifurcated vessel with $\alpha = \beta = 45^{o}$**

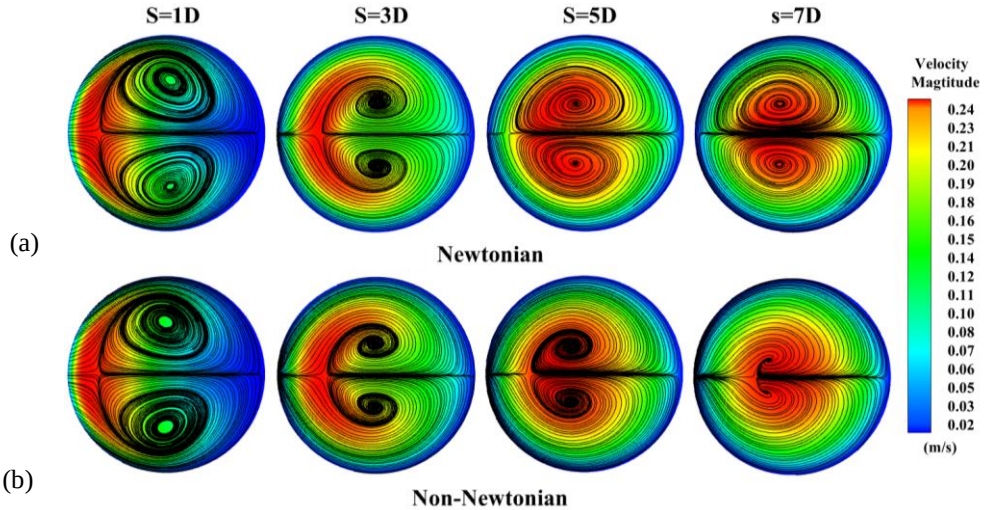


**Fig. 11 Velocity contours and secondary flow streamlines on the cross-sectional planes S=1D, 3D, 5D and 7D for the Newtonian and non-Newtonian flows in the symmetric bifurcated vessel with α=β=45° at the end of diastole.**

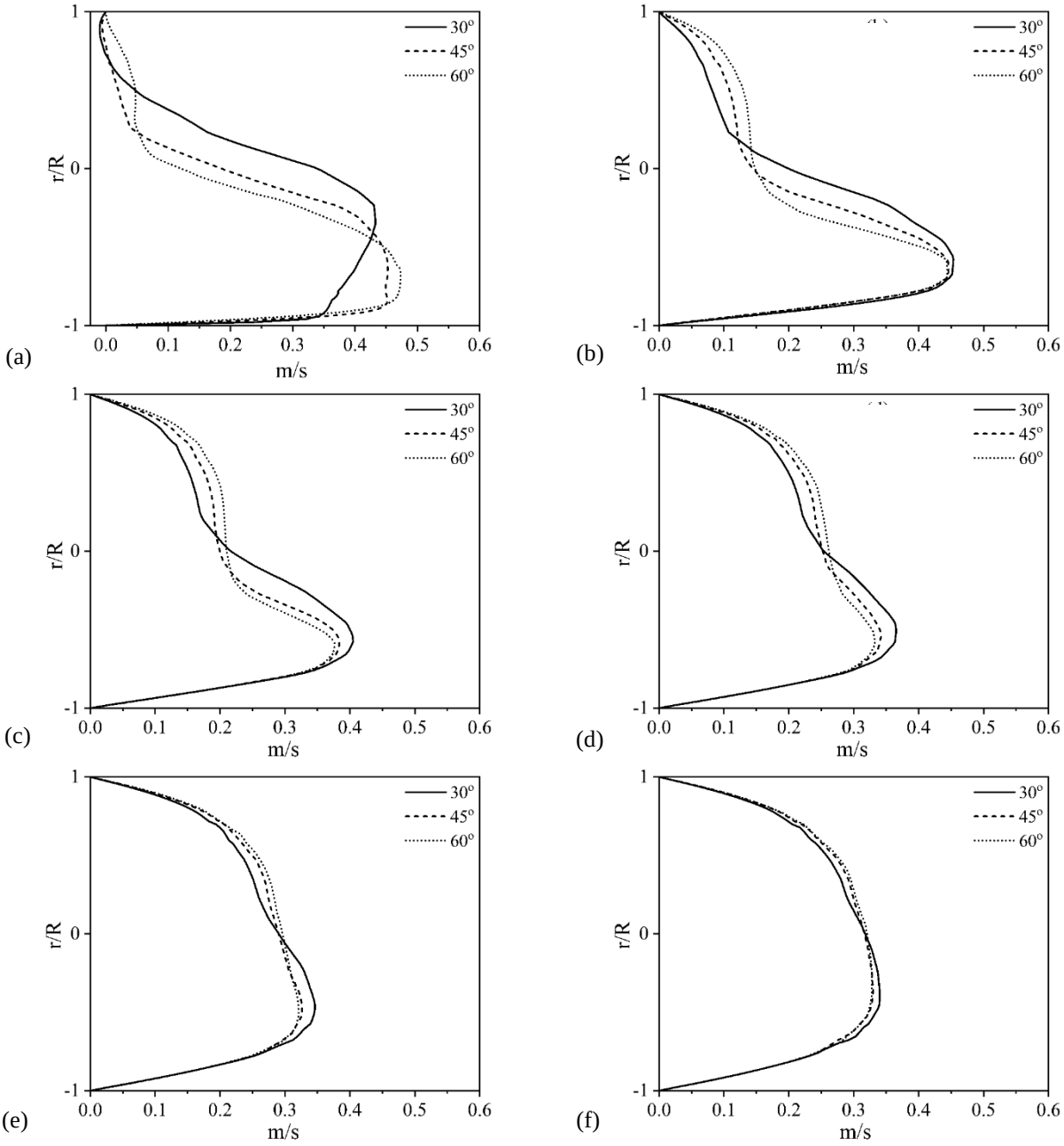


**Fig. 12 Profiles of axial the velocity in the daughter vessel on the bifurcation plane at (a) *S*=1d, (b) *S*=2d, (c) *S*=3d, (d) *S*=4d, (e) *S*=5d, and (f) *S*=6d during the stage of the peak systole for symmetric bifurcated vessels with α = β =30°, 45° and 60°.**

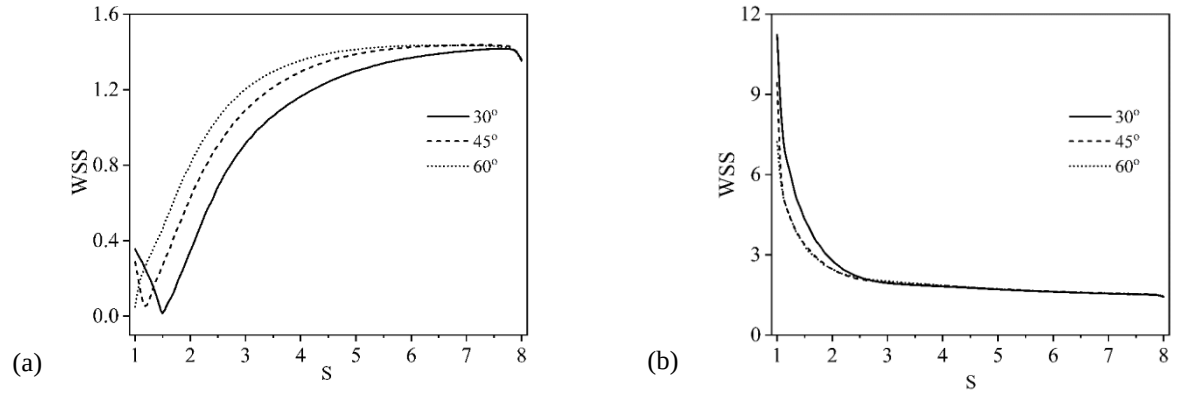


**Fig. 13 Distribution of the WSS along the outer wall (a) and inner wall (b) for the non-Newtonian fluid flow in symmetric bifurcated vessels with α = β = 30°, 45°, and 60°**

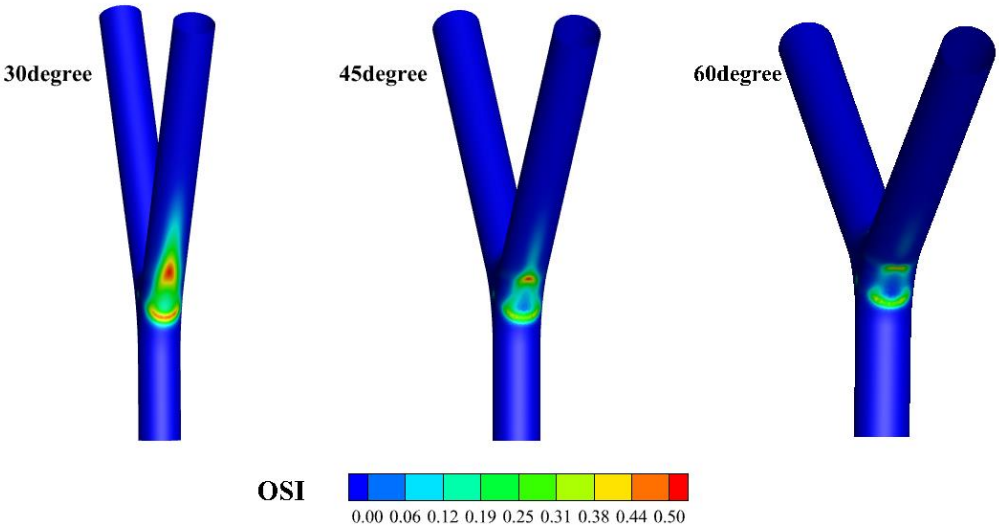


**Fig. 14 TAWSS distributions on the wall of the symmetric bifurcated vessels for the α = β = 30°, 45°, and 60°**

**Table 2 Percentage of the area in low TAWSS zones in the symmetric bifurcated vessels**

| $\alpha = \beta$ | 30° | 45° | 60° |
|---|---|---|---|
| TAWSS(<0.4) | 8.52% | 5.28% | 4.79% |

angle. Figure 13(b) shows the distributions of the WSS along the inner wall of the daughter vessel. Downstream of the apex of the diverging zone, the WSS decreases with an increase in the bifurcation angle. There is an inapparent effect of the bifurcation angle on the WSS after *S*=0.3. As seen in Fig. 12, near the bifurcation, the axial velocity has a greater value near the inner wall than it is near the outer wall. This explains why a high WSS is formed along the inner wall. Meanwhile, the axial velocity profiles are more symmetrical for the high bifurcation angles, which leads to the higher WSS value approaching fully developed flow.

Adel et al. (Pinto & Campos, 2016) demonstrated that zones prone to atherosclerosis had low TAWSS values(<0.4). In symmetrically bifurcated vessels, the larger the bifurcation angle is, the smaller the percentage of this area, as shown in Table 2. The locations of these zones are the same, and they are all on the outer surface of the wall of the bifurcation. Combined with the OSI distribution shown in Fig. 14, and consistent with the conclusions in Table 2, the larger the bifurcation angle is, the smaller the zones with high OSI values.

### 3.4 Effects of Vascular Asymmetry on Blood Flow in the Bifurcated Vessels

The vascular system frequently exhibits an irregularity in the bifurcation angle. To investigate how the flow behavior is impacted by asymmetry in the bifurcation angle, the blood stream for three different bifurcation angles arrangements of 15° - 45°, 30° - 45° and 60° - 45° are investigated. Figure 15 shows the profiles of the axial velocity for the non-Newtonian fluid flow in the asymmetric bifurcated vessels at the peak systole. Under the same flow conditions, the axial velocity profile for the symmetric bifurcated vessel (α = β = 45°) is compared with that for the asymmetric bifurcated vessel. Obviously, in the same asymmetric vessels, the axial velocity for the daughter vessel with a 45° bifurcation angle is larger, which suggests that more fluid enters into the daughter vessel with a higher angle. In addition, it can be deduced that very little reversal flow is observed in the daughter branch with a higher angle, resulting from the larger curvature of the higher angled daughter vessel. These behaviors indicate that blood flow is affected by asymmetry in the bifurcation angle. Blood flow changes greatly with higher bifurcation angles, resulting in a high flow velocity in the daughter vessels. The axial velocity profile for the daughter branch of the symmetric vessel with α=β=45° is almost the same as that for the branch with α = 45° of the asymmetric vessel.

The distributions of the WSS along the outer and inner walls of the three asymmetric bifurcation planes are depicted in Fig. 16 Near the branch point, the WSS on the outer wall of the daughter vessel with larger angles is higher. The WSS along the outer wall of the daughter vessel with a lower angle is nearly 0 at *S*=1, which indicates that flow separation occurs earlier downstream of the daughter vessel. However, comparing Figs 16(b), (d), and (f), it can be observed that the peak WSS decreases while the total bifurcation angle (α+β) increases on the inner wall. This decrease is related to the larger velocity gradient (as shown in Fig. 15a) For asymmetric bifurcation vessels, it is obvious from Table 3 that when α=45°, the larger β is, the smaller the area of low TAWSS. Figure 17 shows the OSI distribution of three different types of asymmetric bifurcation vessels. Comparing the branch vessels with α=45°, the β angle affects the distribution of the OSI. The larger β is, the more dispersed the distribution of the area with high OSIvalues. For bifurcation vessels with a β angle, as with symmetric bifurcation vessels, branch vessels with larger angles have smaller areas of high OSI values. It is observed that the areas for the region of the low-TAWSS with α=β=30° and α=45° and β=15° are almost equal. Therefore, the symmetry of the bifurcation has a small impact on the risk region on the condition that the total bifurcation angle maintains a fixed value.

## 4. Summary and Conclusions

In the present work, the blood flow in three-dimensional symmetric and asymmetric bifurcated vessels was numerically examined. Newtonian and Carreau-Yasuda non-Newtonian fluids were both considered. A pulsatile boundary condition was applied to the inlet. The effects of the viscosity model, bifurcation angle, and asymmetry of the bifurcation angle on the flow field were investigated.

During the pulse cycle, flow separation and secondary flow are observed in the dividing vessels. In the daughter vessel, the axial velocity is skewed to the inner wall and the WSS along the inner wall is higher near the

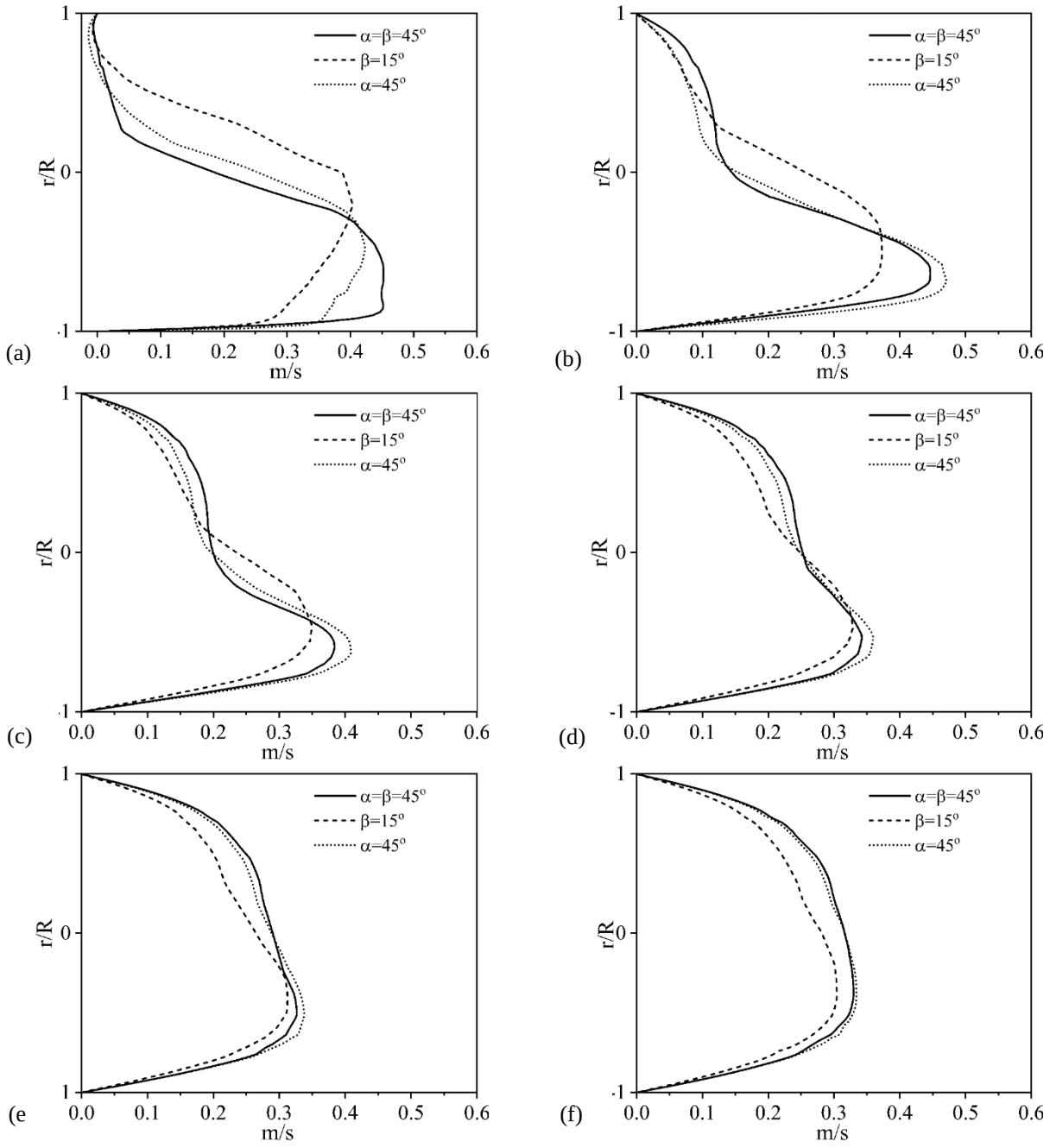


**Fig. 15 Profiles of the axial velocity in the daughter vessel on the bifurcation plane at (a) *S*=1d; (b) *S*=2d; (c) *S*=3d; (d) *S*=4d; (e) *S*=5d and (f) *S*=6d during the stage of the peak systole in the symmetric bifurcated vessel with α = β = 45° and asymmetric bifurcated vessel with α = 45° and β = 15°**

**Table. 3 Percentage of the areas in low TAWSS zones in the asymmetric bifurcated vessels**

| $\alpha \neq \beta$ | $\alpha = 45°,\ \beta = 15°$ | $\alpha = 45°,\ \beta = 30°$ | $\alpha = 45°,\ \beta = 60°$ |
|---|---|---|---|
| TAWSS(<0.4) | 8.49% | 6.71% | 4.45% |

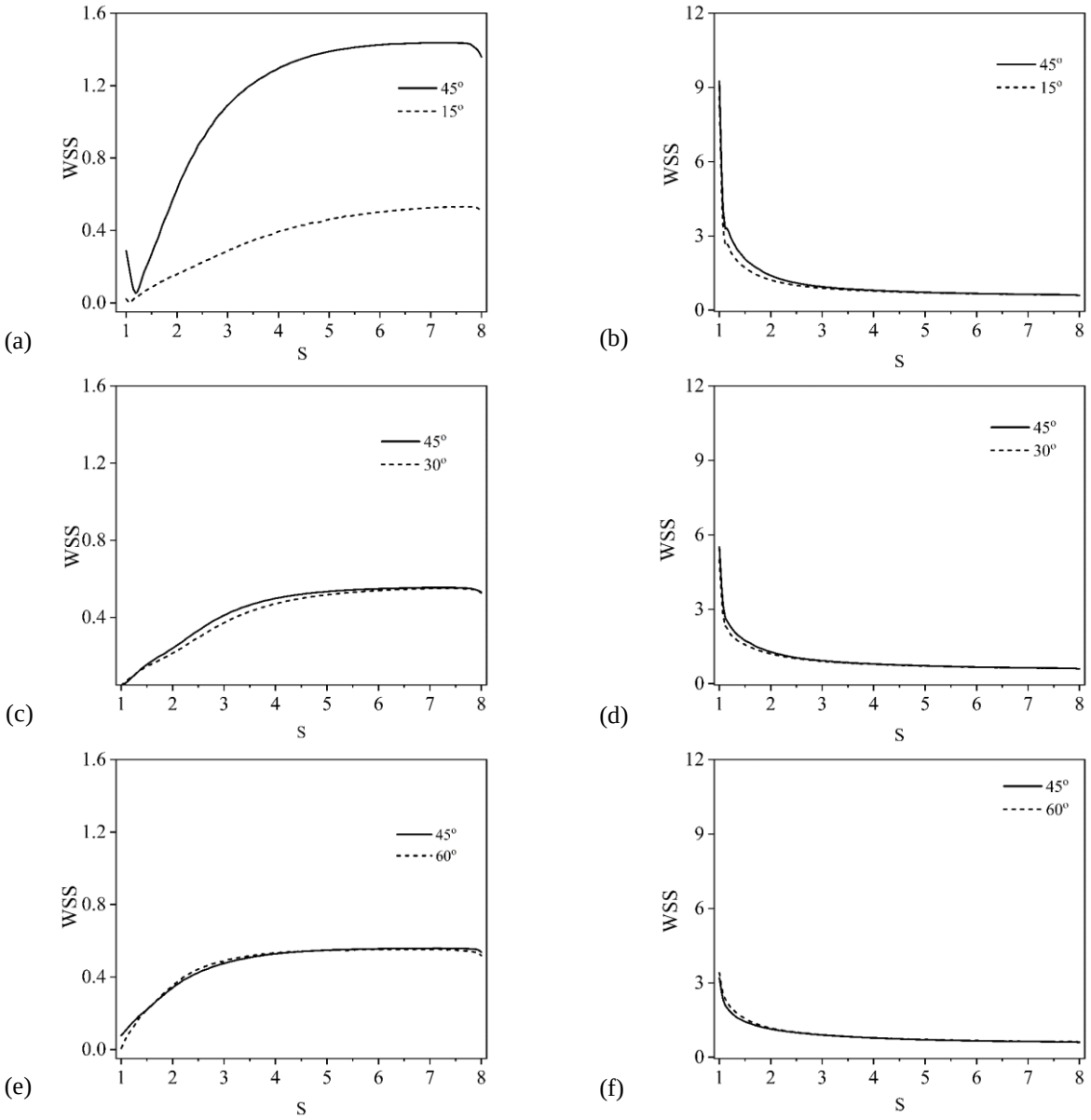


**Fig. 16 Distributions of the WSS along the outer and inner walls of the asymmetric bifurcated vessel on the bifurcation plane for α=45°, β=15° (a, b); α=45°, β=30° (c, d) and α=45°, β=60° (e, f) at the end of diastole**

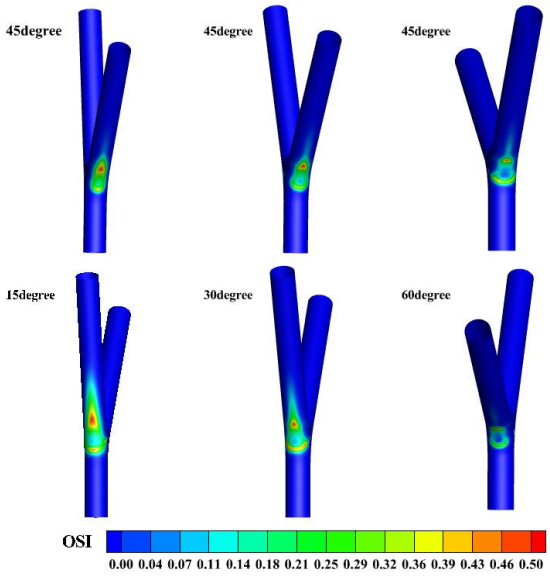


**Fig. 17 TAWSS distributions on the wall of the symmetric bifurcated vessels for the α=45°, β=15°(left); α=45°, β=30°(middle); α=45°, β=60°(right)**

bifurcation due to centripetal acceleration or the pressure gradient initiated by the curvature of the bifurcation. A pair of counter-rotating vortices are observed on the cross-section in the daughter vessel. The effect of the blood viscosity was investigated by comparing results obtained for Newtonian and non-Newtonian fluid flow. The value of the WSS on the outer wall of the daughter branch for the non-Newtonian fluid flow is higher. Additionally, at low flow rates, the secondary flow streamlines of the Newtonian fluid are more pronounced compared to those of non-Newtonian fluid flow in the same zone. Therefore, non-Newtonian properties of blood in bifurcated vessels cannot be ignored at relatively low flow rates. In the symmetric bifurcated vessel, as the bifurcation angle decreases, the peak axial velocity is higher and the magnitude of WSS is lower. In the asymmetric bifurcated vessel, the peak axial velocity for the flow in daughter branch with large angle is greater, and the WSS along the outer wall for which is higher. Moreover, the geometry of the bifurcation has a significant impact on the low-TAWSS and high-OSI regions. The lower the angle of the vessel branch is, the greater the area of the adverse hemodynamic region. The numerical results provide theoretical insight into the mechanism of cardiovascular disease from the aspect of hemodynamics.

## ACKNOWLEDGEMENTS

This work is supported by the National Natural Science Foundation of China (Grant Nos. 11902188, 12002242), Shanghai Science and Technology Talent Program (19YF1417400), and the Fundamental Research Funds for the Central Universities. The grants are gratefully acknowledged.

## CONFLICT OF INTEREST

The authors declare that they have no competing interests

## AUTHORS CONTRIBUTION

**J. Chu**: writing-original draft preparation, data collection, formal analysis. **P.Wei** and **C. S. Lin**: writing-review and editing. **S. Liu**: Methodology, software. **L. L. Xiao**: Supervision, proect, administration. **K. X. Zhang**: methodology.

## REFERENCES

Abugattas, C., Aguirre, A., Castillo, E., & Cruchaga, M. (2020). Numerical study of bifurcation blood flows using three different non-Newtonian constitutive models. *Applied Mathematical Modelling, 88*, 529-549. https://doi.org/10.1016/j.apm.2020.06.066

Arjmandi Tash, O., & Razavi, S. E. (2012). Numerical investigation of pulsatile blood flow in a bifurcation model with a non-planar branch: the effect of different bifurcation angles and non-planar branch. *Bioimpacts*, *2*(4), 195-205. https://doi.org/10.5681/bi.2012.023

Beier, S., Ormiston, J., Webster, M., Cater, J., Norris, S., Medrano-Gracia, P., Young,A., & Cowan, B. (2016). Impact of bifurcation angle and other anatomical characteristics on blood flow - A computational study of non-stented and stented coronary arteries. *Journal of Biomechanics, 49*(9), 1570-1582. https://doi.org/10.1016/j.jbiomech.2016.03.038

Bordones, A. D., Leroux, M., Kheyfets, V. O., Wu, Y. A., Chen, C. Y., & Finol, E. A. (2018). Computational fluid dynamics modeling of the human pulmonary arteries with experimental validation. *Annals of Biomedical Engineering, 46*(9), 1309-1324. https://doi.org/10.1007/s10439-018-2047-1

Caro, C. G., Fitz-Gerald, J. M., & Schroter, R. C. (1969). Arterial wall shear and distribution of early atheroma in man. *Nature*, *223*(5211), 1159-1161. https://doi.org/10.1038/2231159a0

Caballero, A. D., & Laín, S. (2014). Numerical simulation of non-Newtonian blood flow dynamics in human thoracic aorta. *Computer Methods in Biomechanics and Biomedical Engineering, 18*(11), 1200-1216. https://doi.org/10.1080/10255842.2014.887698

Chaichana, T., Sun, Z., & Jewkes, J. (2011). Computation of hemodynamics in the left coronary artery with variable angulations. *Journal of Biomechanics, 44*(10), 1869-1878. https://doi.org/10.1016/j.jbiomech.2011.04.033

Chen, J., & Lu, X. Y. (2004). Numerical investigation of the non-Newtonian blood flow in a bifurcation model with a non-planar branch. *Journal of Biomechanics, 37*(12), 1899-1911. https://doi.org/10.1016/j.jbiomech.2004.02.030

Chen, J., & Lu, X. Y. (2006). Numerical investigation of the non-Newtonian pulsatile blood flow in a bifurcation model with a non-planar branch. *Journal of Biomechanics, 39*(5), 818-832. https://doi.org/10.1016/j.jbiomech.2005.02.003

Chen, Y., Yang, X. L., Iskander, A. J., & Wang, P. (2020). On the flow characteristics in different carotid arteries. *Physics of Fluids, 32*(10), 17. https://doi.org/10.1063/5.0022092

Cox, C., Najjari, M. R., & Plesniak, M. W. (2019). Three-dimensional vortical structures and wall shear stress in a curved artery model. *Physics of Fluids, 31*(12). https://doi.org/10.1063/1.5124876

Freund, J. B. (2014). Numerical simulation of flowing blood cells. *Annual Review of Fluid Mechanics, 46*(1), 67-95. https://doi.org/10.1146/annurev-fluid-010313-141349

Fry, D. L. (2002). Arterial intimal-medial permeability and coevolving structural responses to defined shear-stress exposures. *American Journal of Physiology Heart & Circulatory Physiology, 283*(6), H2341-2355. https://doi.org/10.1152/ajpheart.00219.2001

Gijsen, F. J., Allanic, E., van de Vosse, F. N., & Janssen, J. D. (1999). The influence of the non-Newtonian properties of blood on the flow in large arteries: unsteady flow in a 90 degrees curved tube. *Journal of Biomechanics, 32*(7), 705-713. https://doi.org/10.1016/s0021-9290(99)00014-7

Harris, J., Paul, A., & Ghosh, B. (2023). Numerical simulation of blood flow in aortoiliac bifurcation with increasing degree of stenosis. *Journal of Applied Fluid Mechanics*, *16*(8), 1601-1614. https://doi.org/10.47176/jafm.16.08.1552

Isoda, H., Ohkura, Y., Kosugi, T., Hirano, M., Takeda, H., Hiramatsu, H., Yamashita, S., Takehara, Y., Alley, M., Bammer, R., Pelc, Norbert., Namba, H., & Sakahara, H. (2010). In vivo hemodynamic analysis of intracranial aneurysms obtained by magnetic resonance fluid dynamics (MRFD) based on time-resolved three-dimensional phase-contrast MRI. *Neuroradiology*, *52*(10), 921-928. https://doi.org/10.1007/s00234-009-0635-3

Johnston, B. M., Johnston, P. R., Corney, S., & Kilpatrick, D. (2004). Non-Newtonian blood flow in human right coronary arteries: steady state simulations. *Journal of Biomechanics*, *37*(5), 709-720. https://doi.org/10.1016/j.jbiomech.2003.09.016

Kamangar, S. (2022). Influence of multi stenosis on hemodynamic parameters in an idealized coronary artery model. *Journal of Applied Fluid Mechanics*, *15*(1), 15-23. https://doi.org/10.47176/jafm.15.01.32597

Kannojiya, V., Das, A. K., & Das, P. K. (2021). Simulation of blood as fluid: a review from rheological aspects. *IEEE Reviews in Biomedical Engineering*, *14*, 327-341. https://doi.org/10.1109/RBME.2020.3011182

Kelly, N. S., Gill, H. S., Cookson, A. N., & Fraser, K. H. (2020). Influence of shear-thinning blood rheology on the laminar-turbulent transition over a backward facing step. *Fluids*, *5*(2). https://doi.org/10.3390/fluids5020057

Kucharska-Newton, A., Griswold, M., Yao, Z. H., Foraker, R., Rose, K., Rosamond, W., Wagenknecht, L., Koton, S., Pompeii, L., &. Windham, B. G. (2017). Cardiovascular disease and patterns of change in functional status over 15 years: findings from the atherosclerosis risk in communities (ARIC) study. *Journal of the American Heart Association*, *6*(3). https://doi.org/10.1161/JAHA.116.004144

Libby, P., Ridker, P. M., & Hansson, G. K. (2011). Progress and challenges in translating the biology of atherosclerosis. *Nature*, *473*(7347), 317-325. https://doi.org/10.1038/nature10146

Liu, G., Wu, J., Ghista, D. N., Huang, W., & Wong, K. K. (2015). Hemodynamic characterization of transient blood flow in right coronary arteries with varying curvature and side-branch bifurcation angles. *Computers in Biology and Medicine*, *64*, 117-126. https://doi.org/10.1016/j.compbiomed.2015.06.009

Nagargoje, M., & Gupta, R. (2020). Effect of asymmetry on the flow behavior in an idealized arterial bifurcation. *Computer Methods in Biomechanics and Biomedical Engineering*, *23*(6), 232-247. https://doi.org/10.1080/10255842.2019.1711068

Nagargoje, M. S., Mishra, D. K., & Gupta, R. (2021). Pulsatile flow dynamics in symmetric and asymmetric bifurcating vessels. *Physics of Fluids*, *33*(7), 22. https://doi.org/Artn 07190410.1063/5.0056414

Pinto, S. I., & Campos, J. B. (2016). Numerical study of wall shear stress-based descriptors in the human left coronary artery. *Computer Methods in Biomechanics and Biomedical Engineering*, *19*(13), 1443-1455. https://doi.org/10.1080/10255842.2016.1149575

Soares, A. A., Carvalho, F. A., & Leite, A. (2021). Wall shear stress-based hemodynamic descriptors in the abdominal aorta bifurcation: analysis of a case study. *Journal of Applied Fluid Mechanics*, *14*(6), 1657-1668. https://doi.org/10.47176/jafm.14.06.32319

Spanos, K., Petrocheilou, G., Karathanos, C., Labropoulos, N., Mikhailidis, D., & Giannoukas, A. (2017). Carotid bifurcation geometry and atherosclerosis. *Angiology*, *68*(9), 757-764. https://doi.org/10.1177/0003319716678741

Weddell, J. C., Kwack, J., Imoukhuede, P. I., & Masud, A. (2015). Hemodynamic analysis in an idealized artery tree: differences in wall shear stress between Newtonian and non-Newtonian blood models. *PLoS One*, *10*(4), e0124575. https://doi.org/10.1371/journal.pone.0124575

Xiao, L., Chu, J., Lin, C., Zhang, K., Chen, S., & Yang, L. (2023). Simulation of a tumor cell flowing through a symmetric bifurcated microvessel. *Biomechanics and Modeling in Mechanobiology*, *22*(1), 297-308. https://doi.org/10.1007/s10237-022-01649-3

Xiao, L., Zhang, K., Zhao, J., Chen, S., & Liu, Y. (2021). Viscosity measurement and simulation of microbubble wetting on flat surfaces with many-body dissipative particle dynamics model. *Colloids and Surfaces A: Physicochemical and Engineering Aspects*, *608*. https://doi.org/10.1016/j.colsurfa.2020.125559

Xiao, L. L., Lin, C. S., Chen, S., Liu, Y., Fu, B. M., & Yan, W. W. (2020a). Effects of red blood cell aggregation on the blood flow in a symmetrical stenosed microvessel. *Biomechanics and Modeling in Mechanobiology*, *19*(1), 159-171. https://doi.org/10.1007/s10237-019-01202-9

Xiao, L. L., Song, X. J., & Chen, S. (2020b). Motion of a tumour cell under the blood flow at low Reynolds number in a curved microvessel. *Molecular Simulation*, *47*(1), 1-9. https://doi.org/10.1080/08927022.2020.1856377

Zhang, D., & Dou, K. (2015). Coronary bifurcation intervention: what role do bifurcation angles play? *Journal of Interventional Cardiology*, *28*(3), 236-248. https://doi.org/10.1111/joic.12203

Zhao, S. Z., Xu, X. Y., Hughes, A. D., Thom, S. A., Stanton, A. V., Ariff, B., & Long, Q. (2000). Blood flow and vessel mechanics in a physiologically realistic model of a human carotid arterial bifurcation. *Journal of Biomechanics*, *33*(8), 975-984. https://doi.org/10.1016/s0021-9290(00)00043-9